Restricted Movement of Lipid and Aqueous Dyes through Pores Formed by Influenza Hemagglutinin During Cell Fusion

Joshua Zimmerberg,* Robert Blumenthal,‡ Debi P. Sarkar,‡§ Michael Curran,* and Stephen J. Morris‡‖

* Laboratory of Theoretical and Physical Biology, National Institute of Child Health and Human Development; ‡ Section on Membrane Structure and Function, National Cancer Institute, National Institutes of Health, Bethesda, Maryland 20892; § Department of Biochemistry, University of Delhi, South Campus, New Delhi 110021, India; and ‖ Division of Molecular Biology and Biochemistry, School of Biological Sciences, University of Missouri-Kansas City, Kansas City, Missouri 64110-2499

Abstract. The fusion of cells by influenza hemagglutinin (HA) is the best characterized example of protein-mediated membrane fusion. In simultaneous measurements of pairs of assays for fusion, we determined the order of detectable events during fusion. Fusion pore formation in HA-triggered cell–cell fusion was first detected by changes in cell membrane capacitance, next by a flux of fluorescent lipid, and finally by flux of aqueous fluorescent dye. Fusion pore conductance increased by small steps. A retardation of lipid and aqueous dyes occurred during fusion pore fluctuations. The flux of aqueous dye depended on the size of the molecule. The lack of movement of aqueous dyes while total fusion pore conductance increased suggests that initial HA-triggered fusion events are characterized by the opening of multiple small pores: the formation of a "sieve".

MEMBRANE fusion is an ubiquitous cellular activity which is required for the transfer of materials between membrane-bound compartments in processes such as membrane trafficking, endocytosis and exocytosis (4, 39, 44). Fusion also underlies undesired events such as infection by enveloped viruses (9). Their entry is mediated by fusogenic spike glycoproteins, the best-characterized being influenza hemagglutinin (HA)[1] (4). Previously we have measured membrane and cytoplasmic continuity during fusion of single HA-expressing cells with RBC by monitoring redistribution of lipid and aqueous dyes by video microscopy (31) and flow microspectrofluorometry (18). We observed similar time lags for the onset of fusion with both a lipid dye and a small aqueous dye, NBD-taurine (18, 31). However, the small aqueous dye spread from the labeled RBC to the HA-expressing fibroblast before detectable hemoglobin movement (31). This observation was interpreted to reflect an intermediate structure, the fusion pore, which allows permeation of small molecules but not of large molecules. The magnitude of dye flux was consistent with a number of small pores in the intercellular junction (31).

To obtain detailed information about junctional conductance, patch clamp capacitance measurements (13, 27, 43) have been performed on HA-expressing cells fusing with attached human erythrocytes (RBC) (34, 35, 38). As has been shown for beige mouse mast cell exocytosis (6, 43), fusion of RBC to cells of HA-expressing cell lines is initiated by the formation of a small, partially reversible pore which establishes aqueous continuity of cytoplasm (34, 35, 38). The formation of fusion pores is detected as an increase of conductance and can be measured by the change in junctional admittance. For mast cells, the entire junctional conductance is attributed to a single pore (1, 43); an assumption confirmed by ultrastructural data (10, 29). Increases in junctional conductance are assumed to be due to the widening of this pore. However, electrophysiological techniques can measure only the total junctional conductance, and do not distinguish the number of pores comprising it.

More information on fusion pore structure can be gathered from studies on the permeation of the intercellular fusion junction using different dyes of differing molecular structures. The rate of redistribution of a lipid probe, DiI, was shown to vary by steps (18). This was interpreted as the sequential formation of one fusion pore after another, with a resultant increase in the pathway for lipid flux. A recent publication shows lipid flux to be inhibited in pores less than 0.5 nm in diameter and this is interpreted as support of a gap junction-like initial fusion pore (38).

To determine the number of HA-induced fusion pores which comprise the junctional conductance during fusion, and to determine the relative sequence of dye movements during pore formation, we measured three parameters in pairs; capacitance, membrane-bound dye, and cytoplasmic marker dye, in the fusion of human red cells to HA-

Address all correspondence to J. Zimmerberg, NICHD, NIH, Bldg. 10, Rm. 10D14, Bethesda, MD 10892. Tel.: (301) 496-6571. Fax: (301) 594-0813.

Dr. M. Curran's present address is Dept. of Biology, King College, Bristol, TN 37620.

1. *Abbreviations used in this paper*: HA, hemagglutinin; OMDR, optical memory disk recorder; ROI, region of interest.

expressing fibroblasts. In addition to confirming that lipid dye flux is restricted for early fusion pores, we also find examples of significant aqueous dye retardation in early fusion pores. We find that larger solutes are significantly retarded compared to movement of lipids and small solutes. Fusion pores open in multiple small steps. These findings are consistent with the formation of multiple pores of relatively small diameter.

Materials and Methods

Solutions for the fusion experiments were prepared from PBS (137 mM NaCl, 2.7 mM KCl, 8.1 mM Na_2HPO_4, 1.5 mM KH_2PO_4, pH 7.4) titrated with citric acid to the required pH. Octadecyl rhodamine B chloride (R18), 1,1' dihexadecyl 3,3,3',3' tetramethyl indocarbocyanine perchlorate (DiI), 3,3'dioctadecyloxacarbocyanine perchlorate (DiO), *N*-(7-nitrobenzo-2-oxa-1,3-diazol-4-yl) taurine (NBD-taurine), 5-(and 6)-carboxyfluorescein, carboxy-x-rhodamine, BCECF, calcein, and lucifer yellow dextran, 10 kD, were obtained from Molecular Probes, Inc. (Eugene, OR). Fresh human RBC were obtained from the National Institutes of Health blood bank or directly from normal healthy volunteers and were used within five days. DME^- and DME containing 10% fetal calf serum and penicillin/streptomycin (DME^+) were obtained from Life Technologies, Inc. (Grand Island, NY). Trypsin/EDTA was from GIBCO BRL (Gaithersburg, MD) and neuraminidase was fraction III from Sigma Chem. Co. (St. Louis, MO).

Preparation of Cells

Human RBC were freshly isolated from whole blood and labeled with fluorescent dyes. Soluble dyes carboxyfluorescein, BCECF, carboxy-x-rhodamine or calcein were introduced by lysis and resealing (8, 26) to obtain comparable concentrations; soluble NBD-taurine was loaded as previously described (26, 31). Lucifer yellow dextran was loaded as described (35). Membrane-bound dyes R18, DiI, or DiO were labeled by addition of an ethanolic solution, followed by washing six times. Some cells were double-labeled with one soluble and one membrane bound dye (24, 26). HA-expressing fibroblasts (GP4F) expressing HA from the influenza virus strain A/Japan/305/57(H2N2) were cultured as previously described (12, 25, 31), and discarded after passage 20. Confluent monolayers were split 1:5 and placed for 48 h at 37°C in a 5% CO_2 incubator. For combination fluorescence microscopy/patch clamp experiments, cells were lifted with 0.1% trypsin and 0.04% EDTA, washed 3× with 15 ml DME^- and resuspended at 10^6 cells/ml. 50 μl of GP4F cells were plated onto 2 × 2 cm coverslip in 35-mm petri dishes containing a suspension of 0.005% labeled RBC in PBS with Ca^{2+} and Mg^{2+}. The petri dishes were incubated for 15 min at room temperature with occasional shaking. Microscopic observation determined at which point single RBC were bound to the activated GP4F cells. The cover slips were rinsed in PBS to remove unbound RBC, placed in complete DME^+, and then returned to the CO_2 incubator for 4–8 h. Lifting cells with more trypsin than needed for activation of HA seemed to result in slower development of individual fusion pores.

For double label video microscopy, the cells were lifted with trypsin/EDTA as above, then diluted 1:5 and plated onto no. 00 glass coverslips (Corning Glass, Corning, NY). After two or more days in culture, unless otherwise noted, the cells were activated with trypsin (5 μg/ml) and neuraminidase (220 μg/ml in DME^-) and decorated with RBCs containing one soluble probe and one membrane probe, as described previously (26). Cells were used within 2 h of activation. For experiments comparing calcein to carboxy-x-rhodamine, cells growing in T flasks were activated with 50 μg/ml trypsin and 220 μg/ml neuraminidase, decorated with labeled RBC, then lifted with 500 μg/ml trypsin and 0.02% EDTA, and finally plated onto poly-L-lysine–coated coverslips for microscopic observation (26, 31). The high trypsin treatment used in this last set of experiments led to longer start times.

Multi-wavelength Fluorescence Microscopy

A digital video microscopy imaging system was developed for the simultaneous recording of two different fluorescent dyes as well as phase contrast using an inverted microscope equipped either with two or three intensified CCD video cameras (24, 26). All simultaneous dye measurements were made at 37°C.

After identifying the approximate start time for dye redistribution, 30–90-s segments of video taped data were transferred to an optical memory disk recorder (OMDR) (TQ 3031; Panasonic, Secaucus, NJ). For each fusion event, two region of interest (ROI) masks were created which included the fibroblast but excluded the RBC. For each frame, integrated gray levels in both ROIs were measured. The relative differences in the start of dye redistribution was determined from the changes in slope.

Analyzing the increase in fluorescence in the target fibroblast is more sensitive than trying to distinguish small decreases in RBC fluorescence (38), since both movement of dye from the RBC and photo bleaching will produce apparent decreases in RBC fluorescence. Also, both R18 and DiI can be incorporated into the RBC membrane at self quenching concentrations (18, 25, 31). Thus the kinetics of dye transfer from the RBC to the fibroblast can be distorted by the competing dequenching process.

Stegmann et al. (37) recently reported that the dissociation of self-quenched R18 aggregates may be slow enough to distort the kinetics of the redistribution of this dye. DiI is not subject to this problem (38). If spread of R18 was a notable problem for the experiments reported here, we would have expected to see significantly shorter differences in start times for R18 paired with a given soluble dye compared to DiI paired with the same dye. In fact no such difference was observed (18). A second criticism of R18 is that transfer of dye in the absence of fusion is sometimes observed (38). We never have this problem if we take care to remove unincorporated dye by repeated washings (26). In all of our experiments, the labeled RBC have been in contact with the fibroblasts for minutes to hours before experiments are initiated. In fact, until fusion is triggered, we see no significant difference between R18 fluorescence in the GP4F fibroblasts and background areas containing no cells. To avoid photodamage, 0.03% transmittance neutral density filters were used for excitation and the bath solution contained 1 mM of n-propyl gallate (25, 26).

Simultaneous Patch-Clamp/Fluorescence Imaging

Simultaneous capacitance/video measurements were made on the decorated fibroblasts essentially as described previously (43), except that cell fluorescence was recorded simultaneously with capacitance, as described in detail (41). After recording the fluorescent images and the electrical data on two separate tape recorders, the appropriate segment of image data was transferred to an OMDR as above. An image processor (151; Imaging Technologies, Woburn, MA) was programmed to measure the mean pixel intensity within up to eight ROI (programs available upon request). Mean pixel intensities were measured in three places; (*a*) in background, (*b*) control RBCs (unattached to any fibroblast), and (*c*) RBC attached to the GP4F cell, all within each individual video frame or within linear averages of 2–32 frames. These data were analyzed using commercial software (MATLAB; Mathworks, Natick, MA and Sigmaplot; Jandel Corp., San Rafael, CA). Bleaching and fluctuations in arc lamp intensity were accounted for by dividing the integrated RBC/GP4F average pixel intensity by the integrated RBC average pixel intensity, after subtracting the average background intensity from each.

Whole-cell Capacitance

Capacitance measurements were performed using the technique of Neher and Marty (27), but a stimulating sine wave of 82 or 163 Hz was used to maximize detection of small pores. Junctional conductance can be measured from total capacitance because the red cell membrane capacitance is in series with the fusion pore conductances, and only reaches the final level when the fusion pores are large, as is the case for mast cell exocytosis (34, 41, 43). We used the following equation to calculate fusion pore conductance, derived from the exocytosis of mast cells (41, 43).

$$g_p = \frac{\omega C_{rbc}}{[\omega C_{rbc}/I - 1]^{1/2} - \omega C_{rbc} R_s} \quad (1)$$

where g_p is the fusion pore conductance, $\omega = 2\pi f$, (where f is frequency), I is the measured capacitance for that point, and R_s is the series resistance of the pipette. Standard patch clamp apparatus and amplifiers were used, and capacitance was calibrated with a known change in the C_{slow} compensation. Change of pH was effected by rapid perfusion of a pH 5.1 Ringers solution (21). Briefly, a small, perforated U-tube was placed right above the cell pair, with one end connected to the test solution above the level of the chamber. The other end was held below the level of the chamber. Adjustment of the end of the effluent tube resulted in either suction of media into the hole in the U-tube, or discharge of the test solution onto the cell pair. The temperature was regulated to 37°C (unless otherwise stated) with a

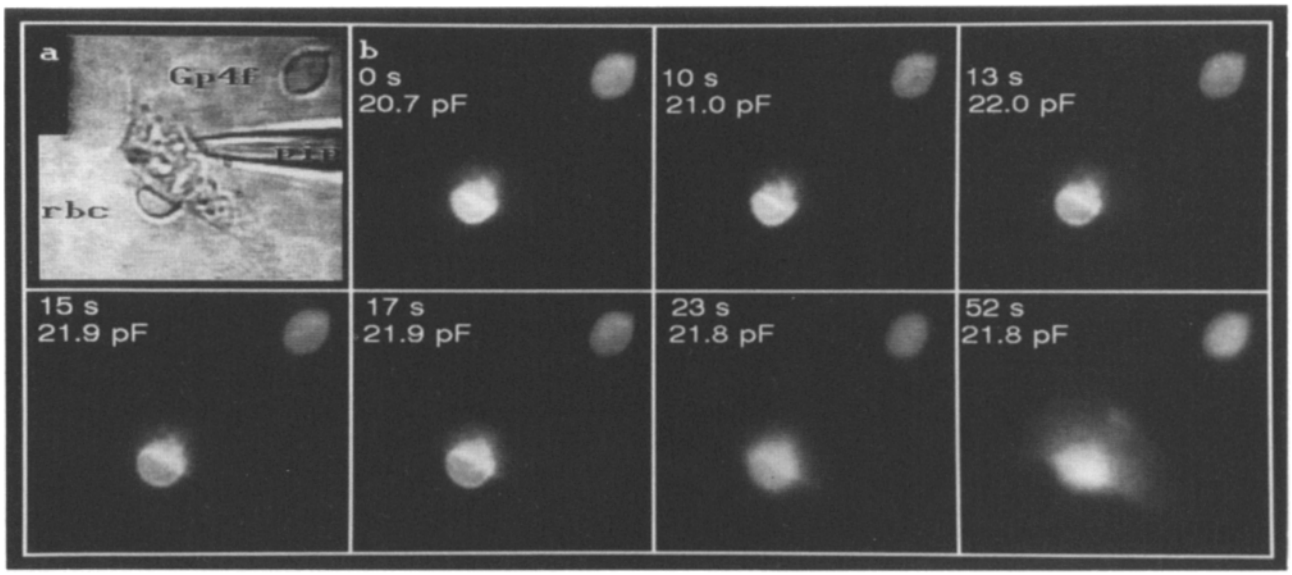

Figure 1. Lipid flux in a fusing RBC-GP4F cell pair. *a* shows a brightfield image of two R18-labeled RBCs attached to a GP4F cell. The patch pipette used for electrical recording is seen to the right. Fluorescent images were recorded at the indicated times after low pH activation. Only the bottom RBC fused with the GP4F cell. Total cell capacitance is shown after fusion increased first by 0.3 pF (total 21 pF), then by a total of 1.3 pF (total 22 pF). At 10 s, fusion pore conductance was 0.4 nS.

Peltier device, where temperature was monitored with a micro-thermistor placed within 50 μm of the GP4F-RBC cell pair to be measured, since a gradient of temperature was found to exist between the edge and center of the glass dish. This thermistor was used to provide a feedback system for the temperature regulation, so that the temperature in the immediate vicinity of the fusing cells was stable.

Results

Detection of Single Fusion Events by Capacitance and Lipid Redistribution.

To obtain detailed information on the time course of fusion of individual pairs of cells, we measured capacitance changes as well as either lipid or aqueous dye transfer using quantitative fluorescence video microscopy. The fusion of an HA-expressing fibroblast (GP4F) with an R18-labeled erythrocyte is shown in Fig. 1. Exposing the GP4F-RBC complex to pH below 5.2 caused spreading of the dye over the surface of the GP4F cell, and concomitant depletion of dye in the RBC membrane (18, 31, 38). The dye redistribution started after a lag time of about 15 s and was complete within 52 s. The total fluorescence dequenching was quantified by integrating pixel intensities over the entire GP4F-RBC area. Fig. 2 *A* shows total fluorescence change in the GP4F-RBC complex as a function of time. Similar curves were seen in the study of single fusion events studied by rapid-flow quantitative fluorescence microscopy (18).

To detect earlier events, we measured out-of-phase admittance, the imaginary portion of the admittance of the fibroblast, which is proportional to the plasma membrane capacitance (Fig. 2). About 9.4 s after activation of HA by acidifying the external medium, capacitance began to increase in successive episodes after an initial reversible flicker. The capacitance change is due to HA-mediated fusion of the RBC with the fibroblast (34). Initially only a small increase in capacitance (0.3 pF) is seen, reflecting the

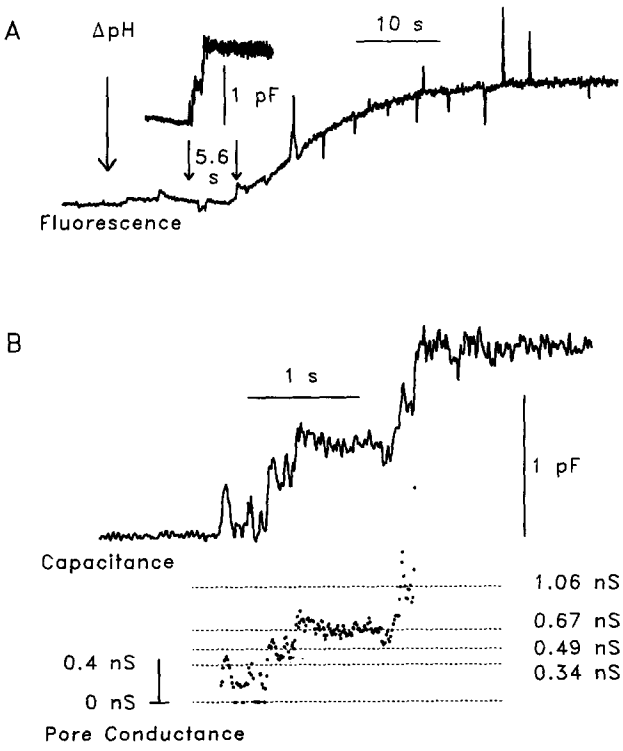

Figure 2. Comparison of membrane flux and junctional conductance (from the cell pair in Fig. 1). (*A*) Top trace: cell capacitance. Bottom trace: Fluorescence change calculated by integrating pixel intensity over the entire RBC-GP4F complex shown in Fig. 1. Arrows (left to right) indicate pH change, onset of capacitance change and onset of fluorescence change. (*B*) (Top and bottom traces: same time scale.) Top trace: cell capacitance, expanded time scale, measured as the imaginary part of the electrical admittance. Extracellular fluid was acidified ~8 s before the start of the trace. The small flicker marks the onset of fusion. Bottom trace: conductance of the HA-mediated electrical connection between the two cells calculated from the capacitance change according to Eq. 1.

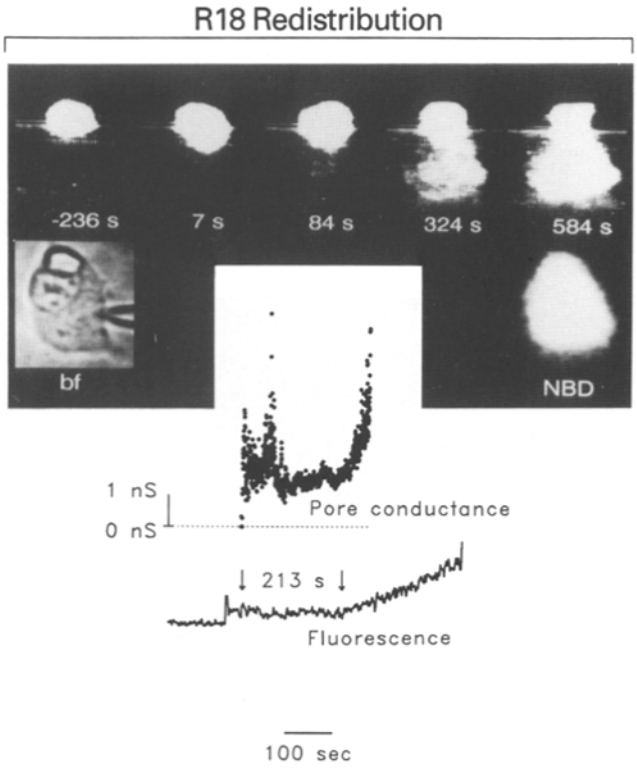

Figure 3. Lipid dye (R18) spread is retarded during fusion pore activity. (*A*) A GP4F cell labeled with R18 and NBD-Taurine was patch-clamped in a fluorescence microscope, as described in the text, then whole cell recording was established and capacitance and series conductance were compensated (16). After setting the phase, capacitance and R18 fluorescence were continuously measured (27). Initial temperature was 31°C. The external solution was acidified for 30 s as described in the text, and then returned to neutral. The chamber was heated 216 s after initial acidification, at 35°C, an abrupt jump in capacitance occurred (0 time), followed by R18 redistribution. At the end of the experiment, (NBD) redistribution was recorded. (*B*) Fusion pore conductance was calculated from capacitance by Eq. 1, and fluorescence in the GP4F cell is plotted on the same axis. Arrows denote onset of capacitance and fluorescence change.

impedance of the fusion pore. The capacitance increase of about 1.3 pF after complete fusion represents the addition of about 130 μm^2 of RBC membrane. This is within the range expected from an RBC, given 1 $\mu F/cm^2$ specific capacitance. The baseline of R18 fluorescence before the capacitance increase was flat, and remained so for ~5.6 s after the first capacitance jump (Fig. 2 *A*).

Capacitance jumps were used to calculate fusion pore formation according to Eq. 1. It is characterized by flicker of pore conductance to ~0.4 nS, followed by a staircase of pore conductances which varied from 0.1–2 nS (Fig. 2 *B*, *bottom*). The total fusion pore conductance became >0.5 nS within 10 s after lowering the pH, but R18 fluorescence changed only 15 s after acid-triggered HA activation. By itself, the staircase of conductance in time is the most direct evidence for small, multiple pores during cell–cell fusion.

Another experiment took place at a lower temperature (31–35°C). Fusion pore formation was initiated a full 4 min after the change of pH. One short flicker was observed, represented in this long time scale as a single point at 0 nS (Fig. 3). A delay of ~213 s after the capacitance increase could be seen before dye redistribution, despite the fusion pore opening to an aggregate size larger than 1.9 nS (Fig. 3).

Detection of Single Fusion Events by Capacitance and Aqueous Dye Redistribution

In contrast to the membrane dye, which redistributed in a sharp gradient, the aqueous dye NBD-taurine redistributed throughout the entire volume of the recipient GP4F cell, in a much broader gradient, reflecting the faster diffusion constant for NBD-taurine and implying that the fusion pore was limiting the diffusion of dye (Fig. 4). The total fluorescence change was quantified by integrating pixel intensities over the entire GP4F area (Fig. 5 *A*). Total fluorescence change in the GP4F cell as a function of time was compared to fusion pore opening (Fig. 5, traces show capacitance and pore conductance, respectively). Fluorescence increases in the GP4F cell could be detected after ~5% of total deviation from base line. This occurred 58 s after the first flicker event, or 38 s after pore conductance reached 1.7 nS. Aqueous dye redistribution in this experiment was slow, with a half-time of 423 s (Fig. 5, *top*). The observed lag time between the capacitance change and detection of NBD-taurine in the HA-expressing fibroblast, indicates that the movement of NBD-taurine through the fusion pore was restricted (see Discussion).

In another experiment, a more typical half-time of redistribution was seen (Fig. 6). Fusion pore formation again is first seen in the conductance trace, then dye redistribution is detected 15 s later. Thus, under the same conditions the fusion

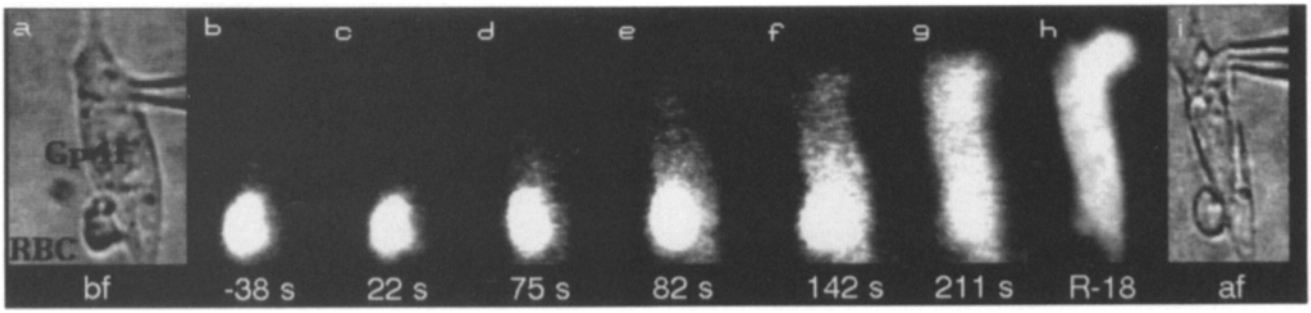

Figure 4. Movement of a small aqueous dye (NBD-taurine) in a fusing RBC-GP4F cell pair. The left and right panels of Fig. 4 show brightfield images of a double-labeled (NBD-taurine and R18) RBC attached to a GP4F cell before and after fusion. The patch pipette used for electrical recording is seen to the right. The panels in between represent NBD fluorescence images recorded at the indicated times (*b–g*). R18 redistribution is shown after fusion (*h*). At 0 time, low pH medium was applied.

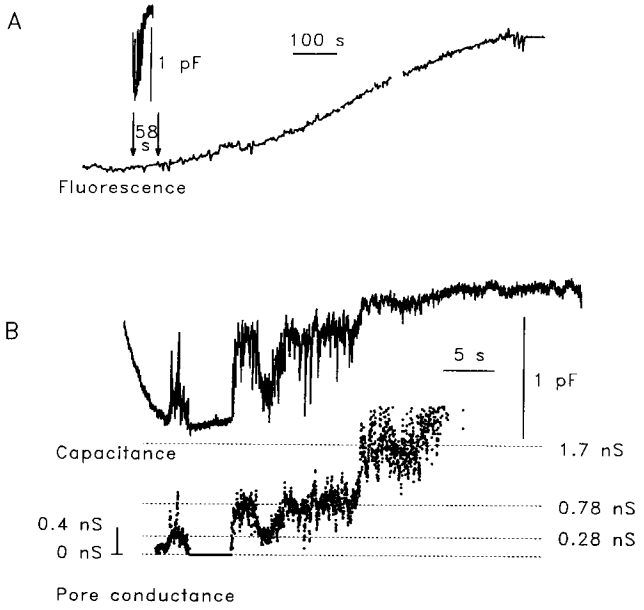

Figure 5. Comparison of aqueous dye permeability and junctional conductance (from the cell pair in Fig. 4). (*A*) Fluorescence change calculated by integrating pixel intensity over the entire GP4F cell. Arrows (left to right) indicate pH change and onset of fluorescence change. Membrane capacitance is shown above (pF scale). (*B*) (Expanded time scale of *A*, *top*). Upper trace: plasma membrane capacitance measured as the imaginary part of the electrical admittance between cytosol and extracellular fluid. The small flicker marks the onset of fusion. Lower trace: Conductance of the HA-mediated electrical connection between the two cells calculated from the capacitance change according to Eq.1. Recording starts 20 s after acidifying the extracellular fluid.

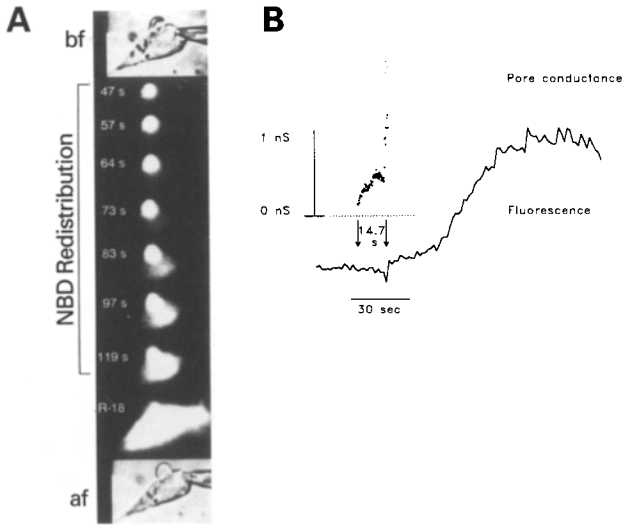

Figure 6. NBD-taurine redistribution in a patch-clamped fibroblast. (*A*) Sequential frames of the fusion of a double-labeled RBC to a GP4F cell expressing HA. Top, before fusion, bright-field image (*bf*). Subsequent images are of NBD fluorescence at the noted times after perfusion with acidic solution. After 2 min, the redistribution of R18 fluorescence was measured (R18). A final brightfield image was obtained after fusion (*af*). (*B*) Fusion pore conductance and fibroblast fluorescence are plotted with the same time scale. Note that the rate of increase of fluorescence abruptly increases when fusion pore conductance rapidly rises above 1.6 nS.

pore can open rapidly following its formation. In such cases, dye redistribution should be a diffusion-limited process, as seen (Fig. 6).

Simultaneous Imaging of Membrane Mixing and Cytoplasmic Mixing

Since movement of both lipid and aqueous dyes can be restricted in the fusion pore formed by influenza HA, we examined the relative movement of one with respect to the other during single fusion events. We used a video microscope (24, 26) which can simultaneously excite two or more vital dyes placed in living cells and image the different emission fluorescence wavelengths on separate cameras, when dye spectra are sufficiently separate. Low pH-triggered fusion of an HA-expressing fibroblast with an RBC double-labeled with R18 and carboxyfluorescein was seen as the redistribution of both dyes (Fig. 7). A single (33 ms) video frame of the three types of images simultaneously acquired (i.e., phase contrast, a membrane dye, and a cytoplasmic marker) is seen at 40 and 79 s after lowering pH. At 40 s there was no movement of dyes, but after 79 s, the soluble dye appeared distributed throughout the fibroblast cytoplasm (Fig. 7 *E*). In contrast, the membrane dye appeared first on the fibroblast in areas just adjacent to the RBC and spread over the cell surface in a wave (Fig. 7 *F, R18*). In part, this is a reflection of the fact that the diffusion constant for R18 is about two orders of magnitude less than for carboxyfluorescein.

The changes in integrated fluorescence levels in the ROI drawn in Fig. 7, *B* and *C* are graphed in Fig. 8 for a 25-s segment of OMDR data starting 35 s after the pH was changed to ~5.0. Frame by frame analysis of the continuous video recording indicates that the start of redistribution of the cytoplasmic dye is retarded compared to the membrane dye.

Table I contains the results of 28 experiments in which the RBC was doubly-labeled with one of each class of dyes, and the redistribution of each dye was detected separately and simultaneously. Table I A shows the time difference between the start of movement of the membrane-bound marker and the cytoplasmic marker (membrane/cytoplasm internal delay) measured as described in the methods section for three different cytoplasmic markers. The cytoplasmic dye never started to move before the membrane dye. Despite the fact that the aqueous dye moves faster (see above), the lipid dye is seen to move first. The probability that the lipid dye would move first in all 28 experiments due to chance is less than 1 in 10^8. Thus there is a relative retardation of the aqueous probe by the fusion pore complex. The lag time between lipid and cytoplasmic movement increased with the molecular weight of the cytoplasmic dye. We tested for significant differences in the membrane/cytoplasmic internal delay interval as a function of the molecular weight of the soluble dye. While there was no significant difference between BCECF and calcein; both of these dyes were significantly slower than carboxyfluorescein (Table I B), as determined by one way analysis of variance. It appears that small differences in size and charge of the cytoplasmic marker correlate

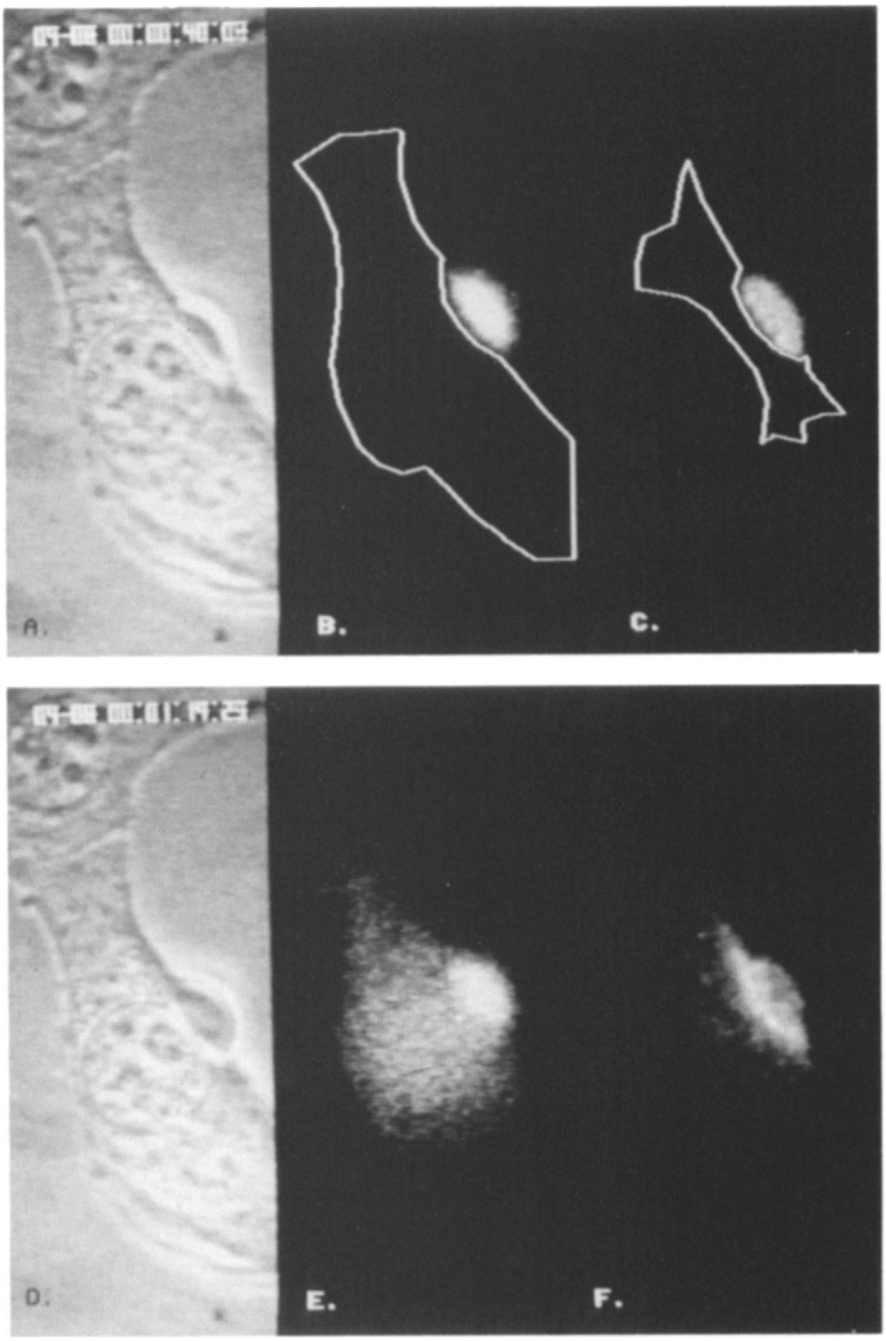

Figure 7. Redistribution of RBC membrane bound (R18) and cytoplasmic (carboxyfluorescein) fluorescent dyes as a result of fusion of a double labeled RBC to a Gp4F fibroblast. Images are of one video frame (33.3 ms). The top row shows (*A*) a phase contrast image, (*B*) carboxyfluorescein fluorescence (480 nm excitation/530 nm emission) and (*C*) R18 fluorescence (565 nm excitation/590 nm emission), taken ~40 s after lowering the pH. This was before the start of fusion as judged by dye redistribution. All three images were taken simultaneously as described (26). The bottom row (*D–F*) contains a similar set of images taken at about 79 s after the pH change. The soluble dye has spread throughout the fibroblast cytoplasm (*E*), while the membrane-bound dye has begun to flow over the fibroblast plasma membrane (*F*).

with large differences in the membrane and cytoplasmic redistribution start times.

To test if charge was the predominant factor in fusion pore permeation for aqueous dyes, we performed separate experiments comparing a new pair of dyes whose spectra did not cross-react, DiO and carboxy-x-rhodamine (MW 535, charge -1) with DiI and calcein (MW 623, charge -4-6). We first ascertained that DiO and DiI had the same lag times, then compared the mean difference in start time for lipid and aqueous dyes: there was no significant difference between carboxy-x-rhodamine and calcein ($P > 0.05$). Thus the fusion pore is relatively nonselective to the degree of negative charge on the permeating species.

In a series of experiments (not shown), RBC ghosts labeled with both 10,000 molecular mass lucifer yellow dextran and DiI fused to GP4F fibroblasts. Although DiI-I redistribution was observed for 5 min, there was no detectable movement of dextran into the fibroblast cytoplasm. However, if cells were examined 9–11 min after the low pH trigger, 30% of cells showing DiI redistribution had detectable dextran movement ($n = 114$). Thus at some point dextran can diffuse into cytoplasm, and dextran is prevented from moving at early times by another barrier, presumably small fusion pores.

Discussion

The low pH triggering of HA starts a complex set of events that ends in the coalescence of membranes and aqueous spaces (5, 8, 32). In this study we focus on the earliest events

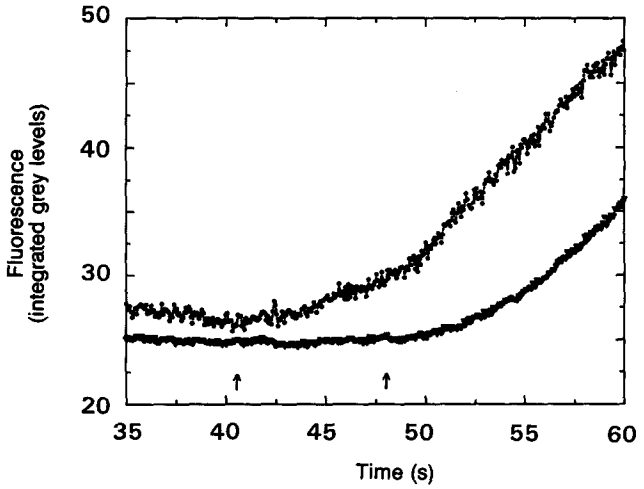

Figure 8. Differences in the start times for lipid and soluble dyes. The pixel intensity of the two regions of interest drawn in Fig. 7, *B* and *C* were integrated as described in Materials and Methods. A 90-s segment of the video taped experiment was transferred to the OMDR for frame by frame analysis. The gray levels for the two ROI's were extracted and saved to an ASCII file. Alternate points are plotted. The start time for each dye was determined as described in the methods section. The difference between start times for this experiment was 7.6 s. (●) R18 (*top line*); (▼) carboxy fluorescein (*bottom line*).

occurring after the initial fusion junction is formed. Whereas in purely lipid membranes, fusion pore opening is complete in hundreds of microseconds (44), in exocytosis fusion pores open, then grow in conductance within 10 ms to a semi-stable stage which corresponds to continuity of membranes (1, 10, 23, 43). In this paper, we have determined the sequence by which measurements of different aspects of HA-mediated cell-cell fusion are first detected: first, aqueous ionic continuity is detected as a change in admittance-reflecting the formation of a small reversible fusion pore of about 0.4 nS. Second, after delays of seconds to minutes, lipid dye flux is seen. Third, aqueous dye flux is seen. The delays between the movement of the lipid and aqueous dyes are a function of the aqueous dye molecule and vary from seconds to minutes. Detection of lipid flux requires significant bulk movement of lipids from one cell to another, so there will always be a delay between the instant of continuity and the detection of flux, as exemplified in our experiments showing the delay between aqueous continuity and aqueous dye flux. The surprising result is that, despite a 100-fold lower diffusion constant for lipids, lipid flux is detected before aqueous dye flux. Since lipid dye spread is never seen before the fusion pore is detected electrically, we believe these results to mean that the junctional conductance is comprised of multiple, small pores.

Lipid and Aqueous Dye Redistribution

Since the random diffusion of materials is governed by the Gaussian distribution, the time to detection of significant flux will be shorter for a dye loaded at a higher concentration, due to a higher signal-to-noise ratio. However, the signal-to-noise ratio was comparable for simultaneously measured lipid and solutes in double-labeled cells. The restricted movement of small aqueous dyes after formation of

Table I. Redistribution of Aqueous Dyes after Fusion Pore Formation

A. Size, charge, and start time differences for soluble dyes, when compared to membrane dyes, for double-labeled red blood cells upon fusion to GP4f cells activated by low trypsin or high trypsin (*).

Fluorescent dye	MW	Charge	Radius	Mean difference in start time
			Å	*s, mean ± SE*
Carboxy Fluorescein	376	−1	5.2	6.56 ± 1.92 (13 exp.)
Calcein	623	−4–6	6.4	14.66 ± 2.44 (8)
BCECF	520	−4	6.1	22.12 ± 2.60 (7)
Lucifer yellow dextran	10,000	0	24	>60 (3)
Calcein*	623	−4–6	6.4	46.4 ± 5.4 (39)
Carboxy-x-rhodamine*	525	−1	6.2	43.8 ± 4.3 (14)

B. Significance of differences between mean start times for various soluble dyes. Start time differences for the three experimental groups were examined by analysis of variance. The differences between means was tested for significance. CF, carboxy fluorescein.

Comparison	Difference in start times	*P* value
	s	
CF vs. calcein	8.66	<0.05
CF vs. BCECF	15.56	<0.001
Calcein vs. BCECF	6.88	NS
Calcein* vs. carboxy-x-rhodamine*	2.6	NS

*High trypsin

fusion pores indicates that each junction is made of a set of small fusion pores. While an alternate hypothesis of one large fusion pore with obstacles to the aqueous dye movement can explain the dye redistribution data, it does not explain the stepwise increases in fusion pore conductance recorded electrophysiologically. An interesting speculation is that each of the small pores may have effective diameters comparable to the molecular dimensions of the larger dyes, producing a sieving effect which may be used to size the fusion pore. Unfortunately, we cannot yet freeze fusion pores into stable conformations to test this more rigorously. Charge differences do not appear to be very important for redistribution. For the largest molecule, 10,000 molecular mass fluorescein dextran, we did not observe redistribution for up to 5 min after the onset of lipid dye movement (Table I), consistent with our observations on hemoglobin (31). However, using other protocols, it is possible to observe redistribution of large molecules from RBC to HA-expressing cells after several minutes (11, 14, 32, 34). The factors governing this final expansion or coalescence of fusion pores to allow large molecules to move are not known.

Lipid Redistribution

Chen et al. (7) have estimated lipid redistribution through a fusion complex joined at a narrow neck. They show that the kinetics of the normalized fluorescence change can be approximated by a single exponential (X_{app}):

$$X_{app}(t) = 1 - e^{(-t/\tau_l)} \quad (2)$$

Fitting Eq. 2 to the data in Fig. 2 (*bottom*) from the onset of the fluorescence increase yields τ_l = 11.6 s (see Fig. 9),

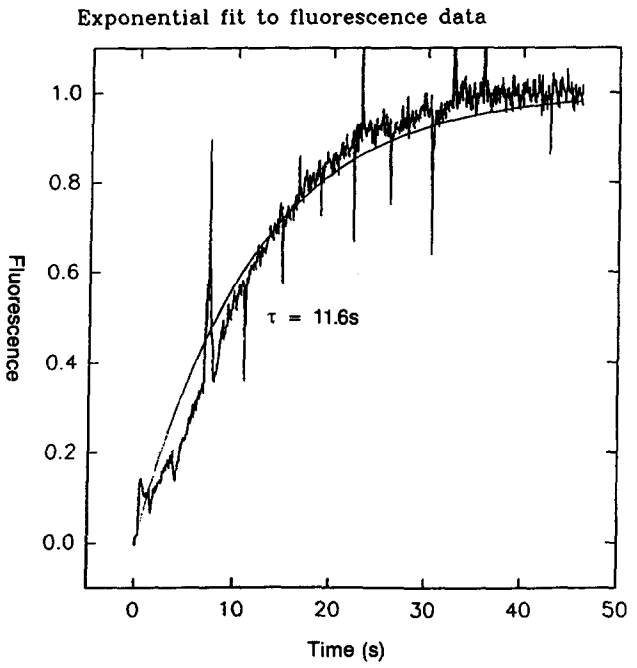

Figure 9. Rate of R18 redistribution following onset of fusion. The fluorescence data from Fig. 2 were normalized according to X = (F − B)/(E − B) where F is fluorescence, B is background fluorescence, and E is fluorescence at equilibrium distribution. The start time was at 15 s. The smooth line is the result of a non-linear curve fit to Eq. 2 with τ = 11.6 s.

where τ_l is for lipidic dye. While the time constant τ_l is a complicated function of the radii of the cells, it is less sensitive to the radius of the pore for single pores (7). The abrupt rise in fluorescence with a single exponential decay argues against the possibility that the lipid dye flux was slow and only gradually rose above the noise: by the time lipid flux is detected, it continues to move rapidly. Rather, we propose that a change in open fusion pore structure suddenly allows lipid dye flux.

In another experiment (Fig. 3), lipid dye motion was obviously restricted for a much longer time. Although lipid flux was not observed until stable fusion pore conductance was higher than 1.7 nS, the initial flickering phase included excursions to aggregate pore conductance in excess of 6 nS. We believe the rapidly fluctuating pore was composed of a number of smaller pores in part because of the larger noise in this experiment.

In fusion mechanisms which feature hemifusion intermediates, there is lipid continuity between the outer monolayers of the contacting membranes before the fusion pore opens. While this lipid continuity implies a pathway for dye diffusion, it is important to remember the difficulties in interpreting the result of restricted lipid flux (44). In particular, domain structures in plasma membrane (30) may restrict dye motion until the rim of the domain is broken. One must also worry about immobilization of lipid dyes. Whereas the establishment of aqueous continuity can be measured as ionic conductivity instantaneously, techniques for measuring lipid continuity are presently restricted to those which require lipid movement, which will always lag behind. However, we confirm and extend the result of Tse et al. (38). Restricted lipid movement during virus-cell fusion has originally been observed by Lowy et al. (22). This restriction may mean that fusion proteins are more intimately involved with lipids than postulated in models where fusion proteins merely bring membranes together so that lipids can interact spontaneously. In lipid/protein mechanisms, protein conformational change drives lipids into fusion intermediates having some features of hemifusion (lipid surfaces of net negative curvature) along with some features of a proteinaceous pore (barrel formation in the plane of the membrane) (42).

Aqueous Dye Redistribution

We performed simultaneous measurements of electrical coupling and dye coupling between an HA-expressing cell fusing with an attached RBC (Figs. 4–6). The situation is similar to observations of gap junction–mediated communication between contiguous cells (3). Coupling between such cells has been characterized by measurement of junctional conductance between isolated pairs of cells by whole-cell recording with two independent patch-clamp circuits. Single channel conductance through gap junction channels range from 50–150 pS (3). Fluorescent dyes have been used to estimate gap junction channel diameter by determining the largest permeable molecule. Those studies indicate that gap junctions are nonselective in their permeability to molecules up to a diameter of 1–1.5 nm (3). Using Langerhans mouse pancreatic beta cells, Perez-Armendariz et al. (28) failed to see dye coupling (lucifer yellow) between pairs of electrically coupled cells. This is similar to the experiment shown in Fig. 4, which indicates electrical coupling between an HA-expressing cell fusing with an RBC under conditions where no dye coupling was observed for 38 s after conductance had reached 1.7 nS. This aggregate conductance of fusion pores is about 10× larger than that of gap junction channels which are permeable to dyes such as NBD-taurine. The question is whether we have sufficient resolution to observe fluorescence changes in the GP4F cell within 38 s.

The expected redistribution time for solutes through a junction between two connecting cells for a given conductance can be estimated from total conductances in a model-independent way. First, the permeability P can be calculated from conductance according to $P = D\rho g$, where D is the diffusion coefficient of the solute and ρ the resistivity of the conducting medium (17). Inserting $D = 5.2 \times 10^{-6}$ cm²/s for NBD-taurine at 37°C and $\rho = 60\ \Omega$ cm for mammalian saline (17), we obtain a permeability coefficient of 5.3×10^{-13} cm³/s at 1.7 nS total conductance. The permeability coefficient is measured according to $P = V\Delta(n2/n0)/\Delta t$ (31), where V is the volume of the RBC and $\Delta(n2/n0)$ is the initial fluorescence change in the HA-expressing cell. The initial change is given by $\Delta t/\tau_a$ (using τ_a for aqueous dyes in Eq. 2) so that $\tau_a = V/P = 234$ s (estimating V at 124 μm³ for a sphere of capacitance 1.2 pF). According to Eq. 2 we would have observed 15% fluorescence change in 38 s through such a pore if motion of the dye were unrestricted, and this was not seen. As opposed to the rapid, abrupt rise in lipid dye fluorescence, the aqueous dye rose slowly, only becoming larger than background noise of 5% after 58 s.

The lack of movement of NBD-taurine in spite of the fact that the fusion pore conductance is continuously increasing (Fig. 4) indicates that the initial fusion event is the opening of multiple small pores. The pore widening that allows larger molecules to move at later stages might either be due to

growth of individual pores or coalescence of pores with each other. These models would explain the large differences seen in start times between ion flow and lipid or soluble fluorescent probe flux. Both multiple pore insertion and pore widening would lead to increased capacitance, with at least the former being an obligate stepwise increase. Because each small pore would be rimmed by lipid, lipid dye flux would increase with the number of small pores, while movement of >300 MW probes would be increasingly restricted. It is possible that the explanation for the variable flux of serotonin seen in different vesicles during the exocytosis of beige mouse mast cells (see reference 2, Fig. 3 *c*) is a variable number and size of fusion pores at the same aggregate conductance. The larger potential area of contact between the large beige granule and the plasma membrane may stimulate multiple dimples and then multiple pores.

Implications for the Structure of the Pore

The fusion pore may be a gap junction–like proteinaceous channel (1) or a funnel-like structure in which the smallest part of the neck is composed of a complex of lipid and *trans*-membrane and fusion peptide portions of HA (15, 33, 36, 42, 44). The finding that cell membrane capacitance increases before lipid movement for small pores, and that larger pores are formed from a series of multiple small pores, means that the smaller fusion pore is a critical structure during membrane fusion. It must be highly permeable to the aqueous ions immediately upon formation to explain the capacitance results. Lipid flux is retarded. While the retardation of lipid flux for small pores would be predicted in proteinaceous channels, it is also possible that only a "funnel" or "neck" between the two cells is purely proteinaceous. Most interesting is the evidence that the transmembrane domains of HA are needed to complete fusion, and these very domains may be retarding the spread of lipid dye as suggested by White et al. (19). In fact, the cytoplasmic tails of HA may aggregate within the lumen of the fusion pore facing the HA-bearing cell's interior, and these tails may obstruct aqueous dye motion. A more detailed analysis of how mutant HA molecules affect the relative dynamics of fusion pore conductance and dye fluxes may yield further insight into mechanisms of HA-mediated membrane fusion.

We would like to thank J. Glass for her help in preparing this manuscript, V. Ratinov for his help with the figures and fusion pore calculations, and J. M. White for her gift of GP4F cells.

Received for publication 10 May 1994 and in revised form 4 October 1994.

References

1. Almers, W., and F. W. Tse. 1990. Transmitter release from synapses: does a preassembled fusion pore initiate exocytosis? *Neuron.* 4:813–818.
2. Alvarez de Toledo, G., R. Fernández-Chacón, and J. M. Fernández. 1993. Release of secretory products during transient vesicle fusion. *Nature (Lond.).* 363:554–558.
3. Bennett, M. V., and V. K. Verselis. 1992. Biophysics of gap junctions. *Semin. Cell Biol.* 3:29–47.
4. Blumenthal, R. 1987. Membrane Fusion. *Curr. Top. Membr. Transp.* 29:203–254.
5. Blumenthal, R., C. Schoch, A. Puri, and M. J. Clague. 1991. A dissection of steps leading to viral envelope protein-mediated membrane fusion. *Ann. NY Acad. Sci.* 635:285–296.
6. Breckenridge, L. J., and W. Almers. 1987. Currents through the fusion pore that forms during exocytosis of a secretory vesicle. *Nature (Lond.).* 328:814–817.
7. Chen, Y., R. J. Rubin, and A. Szabo. 1993. Fluorescence dequenching kinetics of single cell-cell fusion complexes. *Biophys. J.* 65:325–333.
8. Clague, M. J., C. Schoch, and R. Blumenthal. 1991. Delay time for influenza hemagglutinin-induced membrane fusion depends on the hemagglutinin surface density. *J. Virol.* 65:2402–2407.
9. Compans, R. W., A. Helenius, and M. Oldstone. 1989. Cell Biology of Virus Entry, Replication and Pathogenesis. Alan R. Liss, New York. 1–449.
10. Curran, M. J., F. S. Cohen, D. E. Chandler, P. J. Munson, and J. Zimmerberg. 1993. Exocytotic fusion pores exhibit semi-stable states. *J. Membr. Biol.* 133:61–75.
11. Doxsey, S. J., J. Sambrook, A. Helenius, and J. White. 1985. An efficient method for introducing macromolecules into living cells. *J. Cell Biol.* 101:12–27.
12. Ellens, H., J. Bentz, D. Mason, F. Zhang, and J. M. White. 1990. Fusion of influenza hemagglutinin-expressing fibroblasts with glycophorin-bearing liposomes: role of hemagglutinin surface density. *Biochemistry.* 29:9697–9707.
13. Fernandez, J. M., E. Neher, and B. D. Gomperts. 1984. Capacitance measurements reveal stepwise fusion events in degranulating mast cells. *Nature (Lond.).* 312:453–455.
14. Gething, M., R. W. Doms, D. York, and J. White. 1986. Studies on the mechanism of membrane fusion:site-specific mutagenesis of the hemagglutinin of influenza virus. *J. Cell Biol.* 102:11–23.
15. Guy, H. R., S. R. Durell, C. Schoch, and R. Blumenthal. 1992. Analyzing the fusion process of influenza hemagglutinin by mutagenesis and molecular modeling. *Biophys. J.* 62:113–115.
16. Hamill, O. P., A. Marty, E. Neher, B. Sakmann, and F. J. Sigworth. 1981. Improved patch-clamp techniques for high-resolution current recording from cells and cell-free membrane patches. *Pluegers Arch.* 391:85–100.
17. Hille, B. 1992. Ionic Channels of excitable membranes. Sinauer Associates, Sunderland, MA. 291–314.
18. Kaplan, D., J. Zimmerberg, A. Puri, D. P. Sarkar, and R. Blumenthal. 1991. Single cell fusion events induced by influenza hemagglutinin: studies with rapid-flow, quantitative fluorescence microscopy. *Exp. Cell. Res.* 195:137–144.
19. Kemble, G. W., T. Danieli, and J. M. White. 1994. Lipid-anchored influenza hemagglutinin promotes hemifusion, not complete fusion. *Cell.* 76:383–391.
20. Klenk, H.-D., R. Rott, M. Ohrlich, and J. Blodorn. 1975. Activation of influenza A viruses by trypsin treatment. *Virology.* 68:426–439.
21. Krishtal, O. A., and V. I. Pidoplichko. 1980. A receptor for protons in the nerve cell membrane. *Neuroscience.* 5:2325–2327.
22. Lowy, R. J., D. P. Sarkar, Y. Chen, and R. Blumenthal. 1990. Observation of single influenza virus-cell fusion and measurement by fluorescence video microscopy. *Proc. Natl. Acad. Sci. USA.* 87:1850–1854.
23. Monck, J. R., and J. M. Fernandez. 1992. The exocytotic fusion pore. *J. Cell Biol.* 119:1395–1404.
24. Morris, S. J. 1990. Real-time multi-wavelength fluorescence imaging of living cells. *Biotechniques.* 8:296–308.
25. Morris, S. J., D. P. Sarkar, J. M. White, and R. Blumenthal. 1989. Kinetics of pH-dependent fusion between 3T3 fibroblasts expressing influenza hemagglutinin and red blood cells. *J. Biol. Chem.* 264:3972–3978.
26. Morris, S. J., J. Zimmerberg, D. P. Sarkar, and R. Blumenthal. 1993. Kinetics of cell fusion mediated by viral spike glycoproteins. *Methods Enzymol.* 221:42–58.
27. Neher, E., and A. Marty. 1982. Discrete changes of cell membrane capacitance observed under conditions of enhanced secretion in bovine adrenal chromaffin cells. *Proc. Natl. Acad. Sci USA.* 79:6712–6716.
28. Përez-Armendariz, M., C. Roy, D. C. Spray, and M. V. Bennett. 1991. Biophysical properties of gap junctions between freshly dispersed pairs of mouse pancreatic beta cells. *Biophys. J.* 59:76–92.
29. Plattner, H., G. Knoll, and C. Erxleben. 1992. The mechanics of biological membrane fusion. Merger of aspects from electron microscopy and patch-clamp analysis. *J. Cell Sci.* 103:613–618.
30. Rodgers, W., and M. Glaser. 1991. Characterization of lipid domains in erythrocyte membranes. *Proc. Natl. Acad. Sci. USA.* 88:1364–1368.
31. Sarkar, D. P., S. J. Morris, O. Eidelman, J. Zimmerberg, and R. Blumenthal. 1989. Initial stages of influenza hemagglutinin-induced cell fusion monitored simultaneously by two fluorescent events: cytoplasmic continuity and lipid mixing. *J. Cell Biol.* 109:113–122.
32. Schoch, C., and R. Blumenthal. 1993. Role of the fusion peptide sequence in initial stages of influenza hemagglutinin-induced cell fusion. *J. Biol. Chem.* 268:9267–9274.
33. Siegel, D. P. 1993. Modeling protein-induced fusion mechanisms: insights from the relative stability of lipidic structures. *In* Viral Fusion Mechanisms. J. Bentz, editor. CRC Press, Boca Raton, FL. 475–512.
34. Spruce, A. E., A. Iwata, J. M. White, and W. Almers. 1989. Patch clamp studies of single cell-fusion events mediated by a viral fusion protein. *Nature (Lond.).* 342:555–558.
35. Spruce, A. E., A. Iwata, and W. Almers. 1991. The first milliseconds of the pore formed by a fusogenic viral envelope protein during membrane fusion. *Proc. Natl. Acad. Sci. USA.* 88:3623–3627.
36. Stegmann, T., J. M. White, and A. Helenius. 1990. Intermediates in influenza-induced membrane fusion. *EMBO (Eur. Mol. Biol. Organ.) J.* 9:4231–4241.

37. Stegmann, T., P. Schoen, R. Bron, J. Wey, I. Bartoldus, A. Ortiz, J.-L. Nieva, and J. Wilschut. 1993. Evaluation of viral membrane fusion assays. Comparison of the octadecyl rhodamine dequenching assay with the pyrene excimer assay. *Biochemistry.* 32:11330–11337.
38. Tse, F. W., A. Iwata, and W. Almers. 1993. Membrane flux through the pore formed by a fusogenic viral envelope protein during cell fusion. *J. Cell Biol.* 121:543–552.
39. White, J. M. 1992. Membrane fusion. *Science (Wash. DC).* 258:917–924.
40. Wiley, D. C., and J. J. Skehel. 1987. The structure and function of the hemagglutinin membrane glycoprotein of influenza virus. *Annu. Rev. Biochem.* 56:365–394.
41. Zimmerberg, J. 1993. Simultaneous electrical and optical measurements of individual membrane fusion events during exocytosis. *Methods Enzymol.* 221:99–112.
42. Zimmerberg, J., M. Curran, and F. S. Cohen. 1991. A lipid/protein hypothesis for exocytotic fusion pore formation. *Ann. NY Acad. Sci.* 635: 307–317.
43. Zimmerberg, J., M. Curran, F. S. Cohen, and M. Brodwick. 1987. Simultaneous electrical and optical measurements show that membrane fusion precedes secretory granule swelling during exocytosis of beige mouse mast cells. *Proc. Natl. Acad. Sci. USA.* 84:1585–1589.
44. Zimmerberg, J., S. S. Vogel, and L. Chernomordik. 1993. Mechanisms of membrane fusion. *Annu. Rev. Biophys. Biomol. Struct.* 22:433–466.